Geohazard Mechanics 4 (2026) 29–43

Contents lists available at ScienceDirect

Geohazard Mechanics

journal homepage: www.keaipublishing.com/en/journals/geohazard-mechanics

# Geotechnical and geophysical studies for the cause of landslide in Lesalso, Laelay Maichew Wereda, northern Ethiopia

Abadi Gebrehiwot[a,*], Gebremedhin Berhane[b], Yewhalashet Fissha[a,c], Yemane Kide[a], Welegerima Teklay[a], Belaynesh Mekonen[d], Enming Li[e,**]

[a] Faculty of Mines, Aksum University, Aksum, 1010, Ethiopia
[b] School of Earth Sciences, Mekelle University, Mekelle, 231, Ethiopia
[c] Department of Electrical and Computer Engineering, National Institute of Technology, Asahikawa College, Asahikawa city, 071-8142, Japan
[d] Faculty of Water Technology, Aksum University, Aksum, 1010, Ethiopia
[e] Department of Mining Engineering and Earth Sciences, Polytechnic University of Madrid, Madrid, 28003, Spain

ARTICLE INFO

*Keywords:*
Causative factors
Landslide
Soil properties
Vertical electrical sounding

ABSTRACT

The northern highlands of Ethiopia often experience slope failures triggered by rainfall. Landslides are common in Lesalso, Laelay Maichew Wereda, northern Ethiopia, causing destruction to homes, crops, agricultural lands, the death of wildlife, and the eviction of local residents from their homes. The primary objective was to identify the causative and triggering factors for the landslide occurrence. Field investigations, soil laboratory test, vertical electrical sounding (VES) and profiling were conducted. The landslide affected area is characterized by aphanitic basalt with small agglomeratic basalt, phyllite, laterite sandstone, metachert and rhyolite rock units. Physical and engineering properties of 22 soil samples indicated that the failure materials mainly consist of fine grain soils (72.72 %), liquid limit (29.5 %–66.4 %) and plasticity index (7.6 %–43.65 %), medium to high degree of swelling (0.08 %–71.5 %), variable low to high water content (21 %–54.3 %), specific gravity (2.45–2.81), dry unit weight (1.467 g/cm$^3$ to 2.254 g/cm$^3$), activity of soils (0.379 %–1.78 %), soil compression index (0.1785 %–0.43685 %), shrinkage index (0.27 %–28.61 %), shrinkage limit (0.062 %–30.86 %), friction angle ($\phi$) (7.68°–47.94°) and cohesion ($C$) (6.45 kPa–52.72 kPa). The primary factors influencing slope stability include the severely weathered and impermeable rocks beneath the hard and fractured surface, the presence of fine grain soils (clay and silt), a geohydrological setting that facilitates the accumulation of water pressure within the slope, and a steep slope that can generate sufficient stress to induce failure. These findings provide critical insights for the development of proactive mitigation strategies to protect local communities and infrastructure from landslide hazards.

## 1. Introduction

Landslides are prevalent in mountainous and highland areas [1]. Landslides include rock falls, rockslides, debris flows, soil slips, rock avalanches, and mud flows [2]. Ethiopia experienced landslides in 2018 and 2019, resulting in 60 fatalities, 30 household injuries, 5091 displacements, dwelling demolition, and damage to both cultivated and uncultivated lands [3]. Landslides are caused by topography, lithology, geological structures, hydrogeological conditions, land use and cover conditions, rainfall, and other related factors [4]. Rainfall and earthquakes are the primary causes of landslides [5]. Geological structures are crucial to the occurrence of large-scale landslides [6]. Vertical electrical sounding (VES) has been utilized to identify zones of fresh, weathered, and residual soils on landslide bodies [7]. VES is a simple and inexpensive geophysical method that requires little equipment, making it perfect for large-scale surveys [8]. Geotechnical parameters, such as grain size analysis and Atterberg limits, offer crucial data on the grain size distribution, lithology, and moisture content of landslide deposits [9]. Landslides in Tigray, northern Ethiopi, was reported [10]. Understanding engineering properties of the soil is crucial for assessing

* Corresponding author.
** Corresponding author.
*E-mail addresses:* abadidada07@gmail.com (A. Gebrehiwot), enming.li@alumnos.upm.es (E. Li).
Peer review under the responsibility of Liaoning University.

https://doi.org/10.1016/j.ghm.2025.08.005
Received 19 April 2025; Received in revised form 21 May 2025; Accepted 26 August 2025
Available online 28 August 2025

the cause of landslide [11]. A landslide occurred in the northern Ethiopian community of “Lesalso," Laelay Maichew Wereda on August 9, 2020. This caused damage to 7 residential homes and 18 fields of agricultural land. More than 150 people remained in places that could be endangered by landslides, while nearly 15 people have been displaced from the areas destroyed by the landslides; about 25 dwelling homes are at risk, and crops that extend about 8 ha have been destroyed. Nothing is known about the causes, evolutionary trends, or mechanisms of landslides. The aim of this study is to identify causative and triggering factors using a soil laboratory analysis and vertical electrical sounding techniques. Identifying natural and anthropogenic factors associated with landslide triggers is crucial for mitigating future landside risks. In addition, this work provides valuable information to locate safe construction areas in regions that are prone to landslides thus safeguarding lives and property.

## 2. Description of the study area

The study region, which has a total area of approximately 40.7629 km$^2$, is situated in UTM Zone 37, which is bounded by geographic coordinates of 476500–485000 mE longitude and 1555500–1568500 mN latitude (Fig. 1).

The area experiences average annual maximum temperatures (28.9 °C) and minimum temperatures (9.9 °C), with 2018 being the hottest year (Figs. 2 and 3).

May is the hottest month, whereas November is the coldest month [12].

The average annual precipitation in the area is 734.4 mm [12] (Fig. 4).

The study area is characterized by both flat area and mountainous terrain with an elevation range from 2200 to 1850 m above the sea level (Fig. 5). The region's geography is gentle in the eastern and southeastern regions, while it is mountainous and hilly in the north, northwest, west, and southwest. The gradient of the slopes ranges from gentle slopes to steep slopes. The streams are originated from the surrounding highlands. The streams are scarce when the slop is relatively flat and dense where the slop is higher. The drainage pattern of the studied area is mainly determined by dendritic drainage (Fig. 5b). Many of the tributaries are flowing from the northwestern, western and southeastern towards eastern and south eastern parts of the study area. The study area features numerous springs along the aphanetic basalt and shallow groundwater is frequently encountered as indicated by observations made in test pits and shallow wells. Springs can be found in the Lesalso, Seloda and Guemis areas, even during the dry season in May. Along with springs, the area frequently has seepage zones, such as those along asphalt roads and road cuts, which can lead to road saturation.

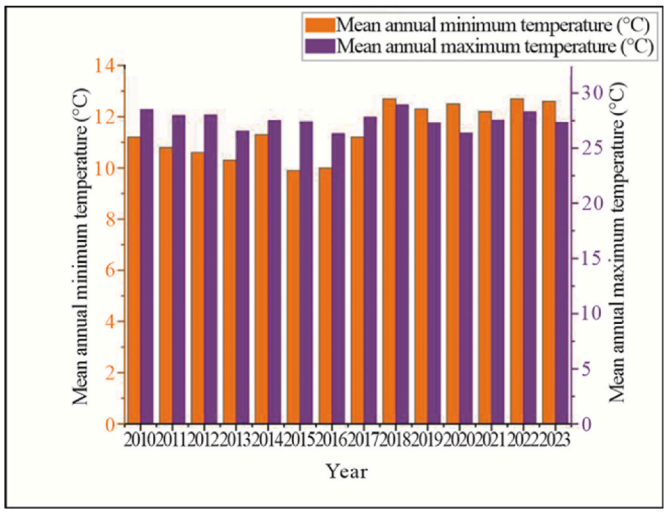


**Fig. 2.** Shows column plots of the maximum and minimum temperature distribution within the year of 2010–2023 [12].

### 2.1. Geology of the study area

Various rock units with varying colors, weathering, strengths, compositions, and structures were used to characterize the study area. The northwest, west, and southwest regions of the study area are exposed to fine-to medium-grained basaltic rock units (Fig. 6). It covered 14.33 km$^2$ (35.37 %) of the total area of 40.675 km$^2$. They range in color from light brown to black. They have a high to moderate degree of weathering and are affected by columnar joints and sub horizontal flows. Of the entire landslide-affected region (6.729 km2), basalt was the most damaged rock unit (36.98 %). Within basalt flows, there are intercalations of volcanic ash and lacustrine deposits. Layering indicates the time gap between lava flow and volcanic eruption. Natali et al. [13] have all shown similar results. Additionally, phyllite and rhyolite rock units made up 4.63 km$^2$ and 0.199 km$^2$ of the region, respectively.

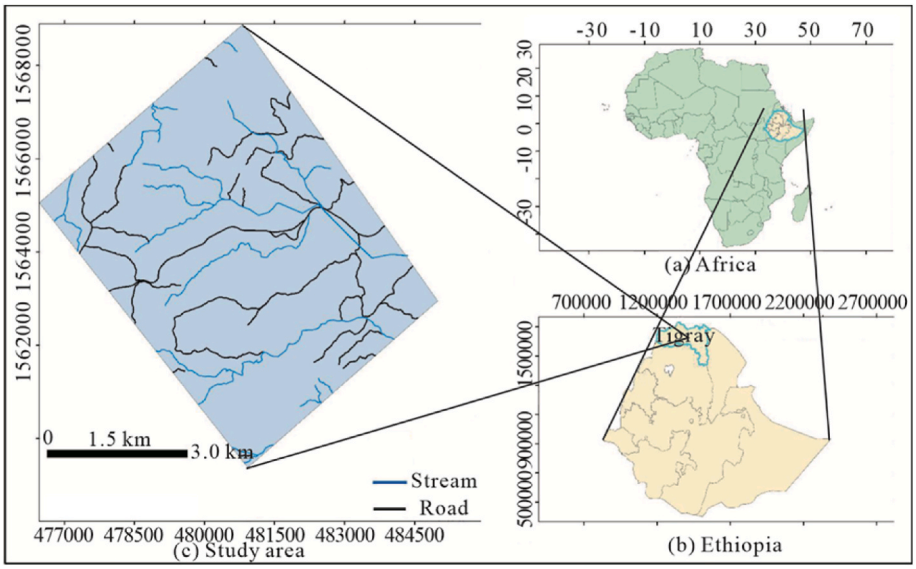


**Fig. 1.** Location map of the study area with respect to Africa, Ethiopia, and Tigray Regional State.

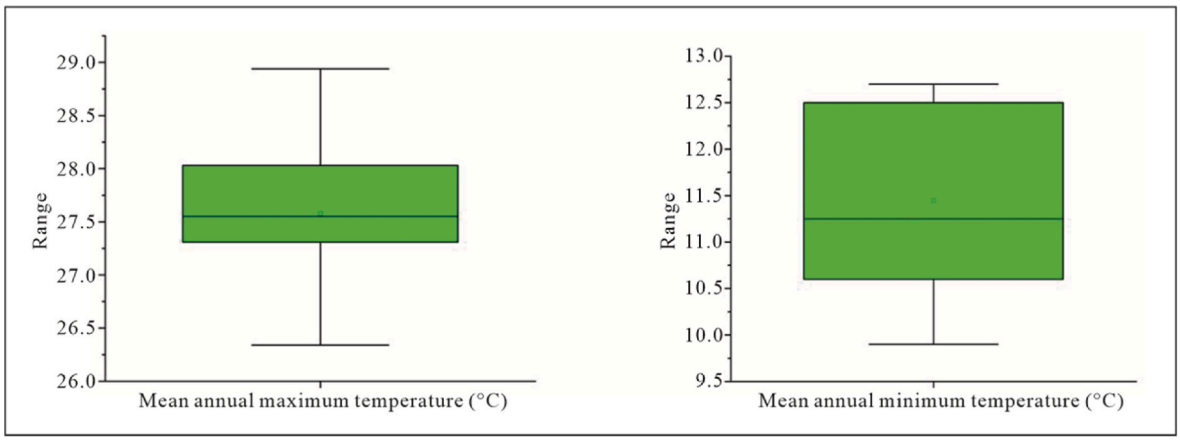


**Fig. 3.** Illustrates the distribution of maximum temperature and minimum temperature within the range interval in quartile box plots style.

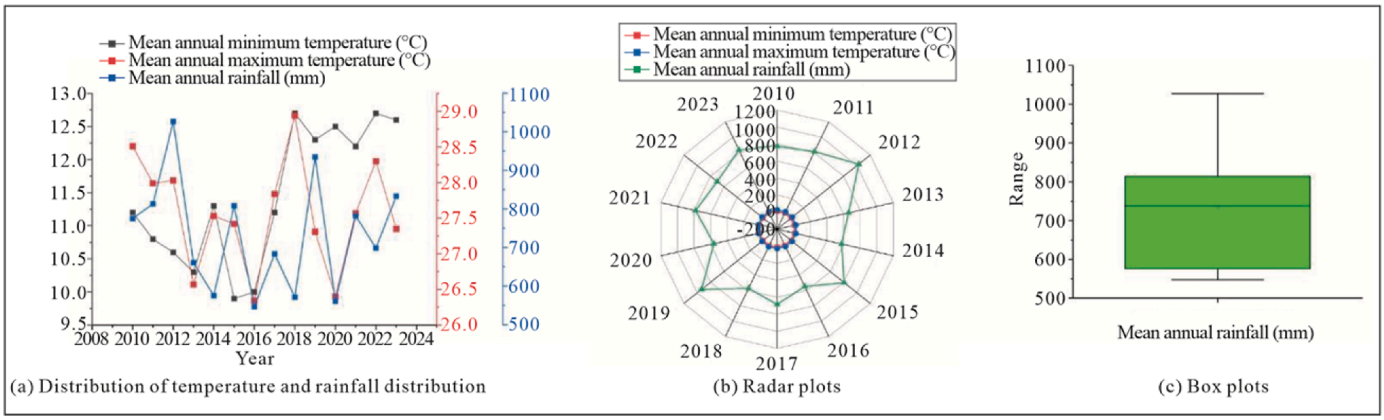


**Fig. 4.** Distribution of temperature and rainfall distribution in 2010–2023.

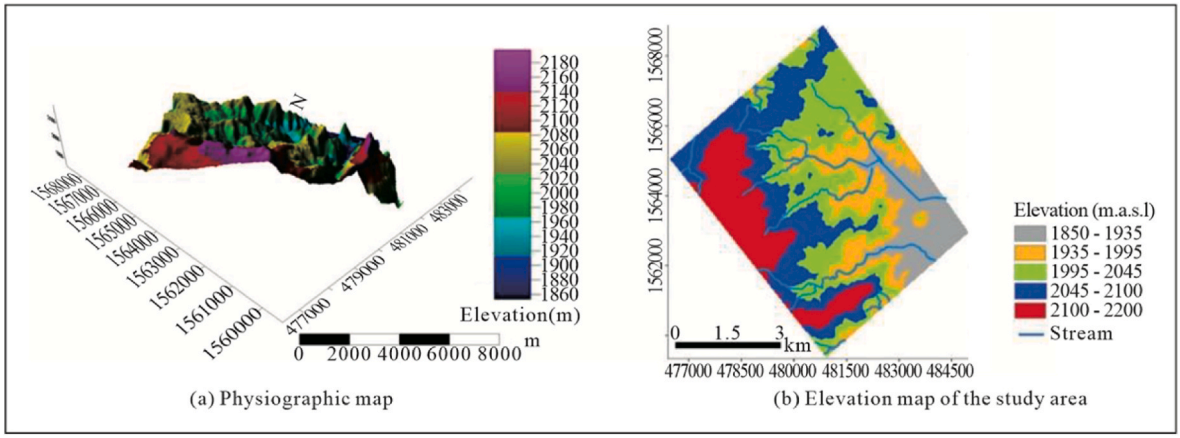


**Fig. 5.** Map of study area.

Agglomeratic basalt rock unit deposits outcrop as river cuts and hillsides. This rock unit is characterized by rounded clasts (rock fragments). It has an agglomerate texture, a fresh grey color, and a weathered red color, and it has a sharp contact with aphanitic basalt. It is mafic in composition and pyroclastic deposits. The southeast, south, and southwest strips of the research area are exposed by phyllite rock unit. Phyllite covered 4.63 km$^2$ of the total area (40.675 km$^2$). These rocks are characterized by different types of local folds, relicts of joints, and are highly weathered, and show a range of colors such as light grey, dark grey, and green (Fig. 7). Phyllite was responsible for 19.075 % of the area landslides. The top highly weathered rock is filled by clay leachates and is expected to have low permeability, but the underlying materials have foliations with N75°W, N44°W, and S15°E orientations, and its joints are oriented S5°W. It is highly deformed with widespread development of slaty cleavage and lineation structure. Similar findings were previously reported by Leulalem et al. [14].

(a) Aphanetic basalt which is highly affected by landslide (b) Compacted agglomeratic basalt (c) Highly weathered basalt

**Fig. 6.** Basaltic rock units.

(a) Highly affected by rock fall landslide and joint (b) Highly jointed exposed due to road cut due to river cut (c) Highly affected by debris flow landslide exposed

**Fig. 7.** Phyllite rock units.

The metachert rock unit extends towards the north, northeast, northwest, south, southeast, and east of the study area. Metachert covered 13.25 $km^2$ (32.71 %) of the 40.675 $km^2$ of the total area. It is grey to light grey in color with very fine texture. These rocks are compact, tiny, and colour banded. Metachert accounted for 18.21 % of the landslides. This rock unit has joints with an N77°W orientation (Fig. 8). Over 95 % of it is made up of fine-grained to cryptocrystalline silica, with small quantities of iron oxide, sericite, and plagioclase. The findings by Leulalem et al. [14] are likewise comparable.

In the research area, laterite sandstone is exposed in the northern, northwest, western, and south western regions. It covered 8.1 $km^2$ of the 40.675 $km^2$ of the total area. This sandstone is quite mature, well-sorted, fine to medium-grained, and reddish-light in color (Fig. 9). It is composed of iron, and is hard and compacted. It has an average thickness of around 40 m in the area. Its red color is a result of iron cement with somewhat sorted particles. Teklebrhan et al. [15] reported similar results. Laterite sandstone accounted for 23.66 % of all landslides.

A rhyolitic rock unit was found and extensively studied in the area. It covered 0.199 $km^2$ of the region (40.675 $km^2$). Rhyolite has a light color with different tones of the same light grey or pink, with oxidation in some areas. Purplish or brick coloring is also sometimes observed. The rock displays a porphyritic texture with larger phenocrysts of quartz and feldspar contained within a fine-grained, aphanitic groundmass, suggesting some rapid cooling at the surface. Mineralogically, rhyolite is composed of quartz, plagioclase, and alkali feldspar, with a small amount of biotite. Moderate weathering results in knobby, erosion-resistant outcrops and the formation of a pale, clay-enriched rind on exposed surfaces. Rhyolite comprised 2.08 % of the total landslides.

### 2.2. Geological structures of the study area

In the study area, there appear primary structures and secondary structures such as bedding plane, fractures (fault and joint), foliation intrusions of sill which were identified from field observation. Details of these different geological structures are discussed as follows.

(a) Highly weathered and affected with landslide (b) Highly compacted with having different set of joints (c) Compacted exposed due to river cut

**Fig. 8.** Metachert rock units.

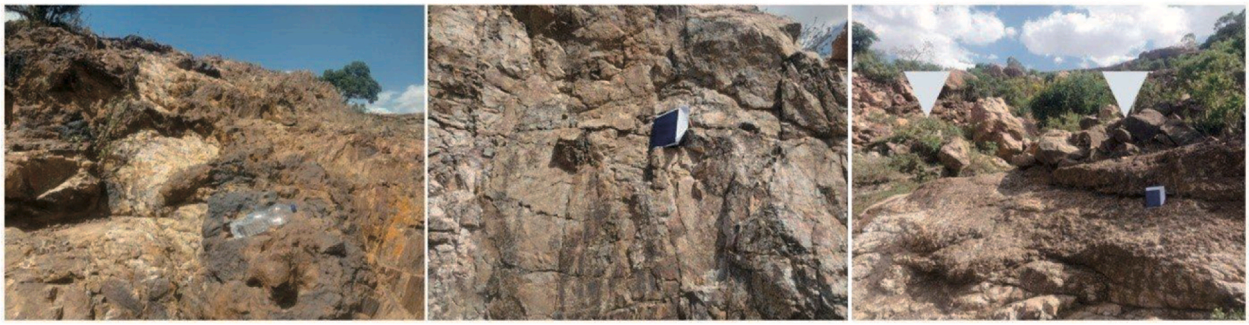

(a) Highly weathered (b) Highly affected by joints which leads to rock fall landslide (c) Highly affected by rock fall landslide

**Fig. 9.** Laterite sandstone rock units.

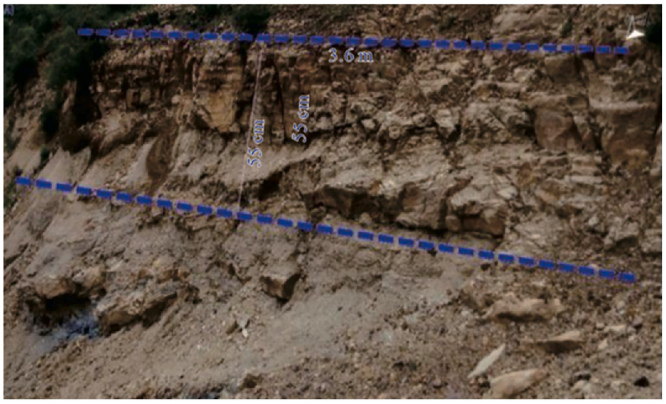


**Fig. 10.** Bedding plane along lateritic sandstone rock unit.

**Fig. 12.** Minor faults along lateritic sandstone rock unit.

### 2.2.1. *Bedding plane*

Bedding plane is exposed in the laterite sandstone with its thickness ranges from 0.5 to 1.2 m (Fig. 10).

### 2.2.2. *Joints*

Joint sets are observed at the phyllite, aphanitic basalt and laterite sandstone. Many joint measurements were taken in the aphanitic basalt, laterite sandstone and phyllite rock units of the study area. The nature of the joint spacing in all the rock units was not uniform everywhere. The aphanitic basalt rock unit is locally massive and affected by very widely spaced systematic joints and columnar joints (Fig. 11).

### 2.2.3. *Fault*

From field observation, minor faults were exposed in the study.

(a) Joint sets (b) Joint with irregular fractures (c) Columnar joint (d) Joint with high aperture in laterite sandstone

**Fig. 11.** Joints in aphanitic basalt.

Along the laterite sandstone rock units, faults which trends to the 355°/65°/NE with throw and heave of 0.5 and 0.3 m respectively and 325°/80°/SW with throw and heave of approximately 1 and 0.6 m respectively were investigated (Fig. 12).

#### 2.2.4. Foliation

Phyllite rock units of the study area were affected by well-developed penetrative foliation. It is characterized by grey color, fine to medium grained and highly to moderately weathered (Fig. 13).

#### 2.2.5. Sill

In the study area, the sill is composed of aphanitic basalt, which is overlain by laterite sandstone. This intrusion is exposed because of hill side (Fig. 14).

**Fig. 14.** Sill intrusion in aphanitic basalt rock unit.

### 2.3. Land use/land cover and soil of the area

Fig. 15 shows the maps of the area. The majority of the land, or 26.29 $km^2$ (64.64 %), was used for agriculture, while 9.329 $km^2$ (22.93 %) was left bare land. However, 10.97 % (4.46 $km^2$), 1.304 % (0.53 $km^2$), and 0.1462 % (0.0595 $km^2$) of the area was covered with grassland, shrub land, and settlements, respectively (Fig. 15b). The landslide had significant effects on both bare land and agricultural land use, accounting for 30.59 % and 29.765 % of the total area, respectively. This result is linked with soil saturation caused by irrigation, soil erosion, and deforestation [16]. Within the study area, 1.42062 $km^2$ (1.11 %) and 1.247 $km^2$ (18.53 %) of the landslides that were inventoried occurred in shrub land and grass land, respectively. Vegetation reduces the likelihood of landslides because plant roots increase the soil's shearing strength by providing mechanical support [17]. Soils of the area was reclassified as leptic regosol, skeletic regosol, vertic luvisol, and haplic cambisol. From soil classes found in the area, vertic luvisol occupied 30.589 $km^2$ (75.565 %) of the area. Others, like haplic cambisol, skeletic regosol, and leptic regosol, cover 4.3467 $km^2$ (10.7379 %), 4.2582 $km^2$ (10.52 %), and 1.286 $km^2$ (3.1785 %) of the area, respectively (Fig. 15c).

## 3. Methodology

### 3.1. Field survey and sampling

Geological mapping, discontinuity surveying, and soil sampling were conducted using field observations, Google Earth Image 2023, and a 1:50,000 scale map of the Aksum region. ArcGIS software/geoprocessing/editor was used to digitize each rock unit. The land use/cover of the area was mapped using a field survey and a 2023 Google Earth image. The soil map of the area was created using ArcGIS 10.4.1/ digitization from the FAO soil map of Tigray, aided by a field survey and literature review. Geological materials in this field are described according to their thickness, color, orientation, and degree of weathering. To ascertain the geotechnical properties of the soil in the research region, 22 soil samples were collected between October and November 2020 under dry weather conditions using the standards in study by Baldwin and Gosling [18]. The sampling pits (sites) were selected at random in landslide-prone sites, and their coordinates were recorded using Global Positioning System (GPS) (Table 1).

The samples were primarily collected from the landslide materials for laboratory testing. Samples were collected and packaged in sterile polyethylene bags, labeled, and air-dried before being brought to the laboratory (Fig. 16).

### 3.2. Soil laboratory test

The liquid limit (*LL*) of the soil is the point where the water content increases, measured using a Casagrande cup [19]. The plasticity of a soil is measured by the plasticity index (*PI*), which indicates the range of water content at which it exhibits plastic qualities. This was calculated using Eq. (1).

$$PI = LL - PL \tag{1}$$

where *PI* is plastic index; *LL* is the liquid limit; and *PL* is plastic limit.

The water content of the soil samples was assessed using the oven-drying method [20]. The soil samples were wet and dried in an oven at 105 °C for 24 h, and the water content was determined by calculating the weight difference after drying according to Eq. (2).

**Fig. 13.** Foliations along phyllite rock unit.

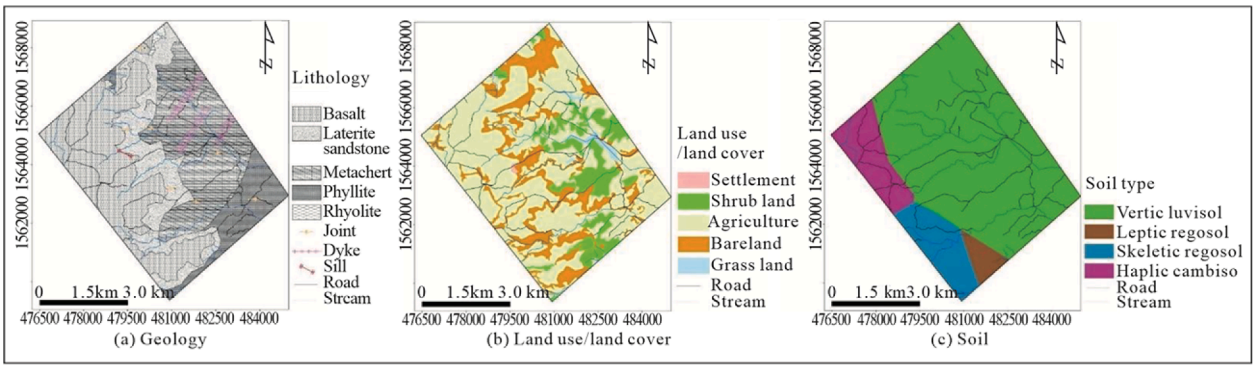


**Fig. 15.** Maps of the area.

**Table 1**
GPS coordinates of soil sampling.

| Ser. No. | Test pit designation | Depth of sampling (m) | GPS location | | |
|---|---|---|---|---|---|
| | | | Longitude (m) | Latitude (m) | Elevation (m) |
| 1 | RH-22 | 1.5 | 0481063 | 1563830 | 1980 |
| 2 | Du-19 | 1.5 | 0481923 | 1563263 | 1998 |
| 3 | Du-18 | 2.0 | 0481994 | 1564053 | 1937 |
| 4 | La-4 | 1.5 | 0480613 | 1565104 | 1953 |
| 5 | Ls-11 | 2.5 | 0478799 | 1564827 | 2101 |
| 6 | Ls-9 | 1.5 | 0479010 | 1565361 | 2030 |
| 7 | Rh-21 | 1.5 | 0481264 | 1563641 | 1969 |
| 8 | MAK-10 | 2.0 | 0478937 | 1565054 | 2077 |
| 9 | Msh-17 | 1.5 | 0481982 | 1564357 | 1960 |
| 10 | Rh-23 | 1.5 | 0480339 | 1563890 | 2010 |
| 11 | Ls-8 | 2.0 | 0479554 | 1565329 | 1996 |
| 12 | Msh-1 | 2.0 | 0482158 | 1565242 | 1934 |
| 13 | La-6 | 2.5 | 0480010 | 1564647 | 1997 |
| 14 | Ls-12 | 2.0 | 0478799 | 1564827 | 2101 |
| 15 | Ls-14 | 2.0 | 0478767 | 1564227 | 2116 |
| 16 | Du-20 | 1.5 | 0481508 | 1563501 | 2019 |
| 17 | Msh-2 | 1.5 | 0481271 | 1565386 | 1969 |
| 18 | Ls-5 | 2.0 | 0479928 | 1564883 | 1982 |
| 19 | Ls-16 | 2.0 | 0478929 | 1563758 | 2124 |
| 20 | Ls-13 | 2.5 | 0478801 | 1564197 | 2108 |
| 21 | Ls-15 | 1.5 | 0476828 | 1564260 | 2121 |
| 22 | Msh-3 | 1.5 | 0480804 | 1564893 | 1960 |

$$\text{Water content}(\%) = \frac{M_W}{M_{ds}} \tag{2}$$

where $M_w$ is mass of water; and $M_{ds}$ is mass of dry soils.

To assess collapsibility, the collapsibility index ($K$) was calculated using Eq. (3).

$$K = \frac{W - LL}{LL - PL} \tag{3}$$

where $w$ is the natural moisture content; $LL$ is the liquid limit; and $PL$ is the plastic limit.

The liquidity index ($LI$) and plasticity index ($PI$) are calculated using the measured Atterberg limits. Eq. (4) is used to calculate the liquidity index ($LI$).

$$LI = \frac{W - PL}{PI} \tag{4}$$

where $PI$ is the plasticity index; $W$ is the water content; and $PL$ is the plastic limit. Eq. (5) was used to determine the consistency index ($CI$).

$$CI = \frac{LL - W}{PI} \tag{5}$$

where $LL$ is the liquid limit; $W$ *is the* water content; and $PI$ is the plasticity index.

The soil compression index of the study area was determined using Eq. (6).

$$C_{c=0.007(LL-10)} \tag{6}$$

where $LL$ is the liquid limit.

A specific gravity test was conducted using a pycnometer [21]. The shrinkage limits of the 22 soils were determined using the procedure [22]. The shrinkage index was calculated using Eq. (7).

$$\text{Shrinkage index}\left(I_{s=\text{Plastic limit}-\text{Shrinkage limit}}\right) \tag{7}$$

The soil activity was calculated using Eq. (8).

$$\text{Activity of soil} = \frac{\text{Plasticity index}(PI)}{\%\text{ clay fraction}} \tag{8}$$

The free swell was predicted using Eq. (9).

$$\text{Free swell } (FS) = \left(\frac{V_{W-V_K}}{V_K}\right) \times 100 \tag{9}$$

where $V_W$ is the sample level in water; and $V_K$ is the sample level in kerosene.

Direct shear testing of the 22 soil samples was performed in compliance with the study [23].

**Fig. 16.** Field soil sampling.

(a) Vertical electrical sounding (b) Vertical electrical sounding (c) Profiling

**Fig. 17.** Field work.

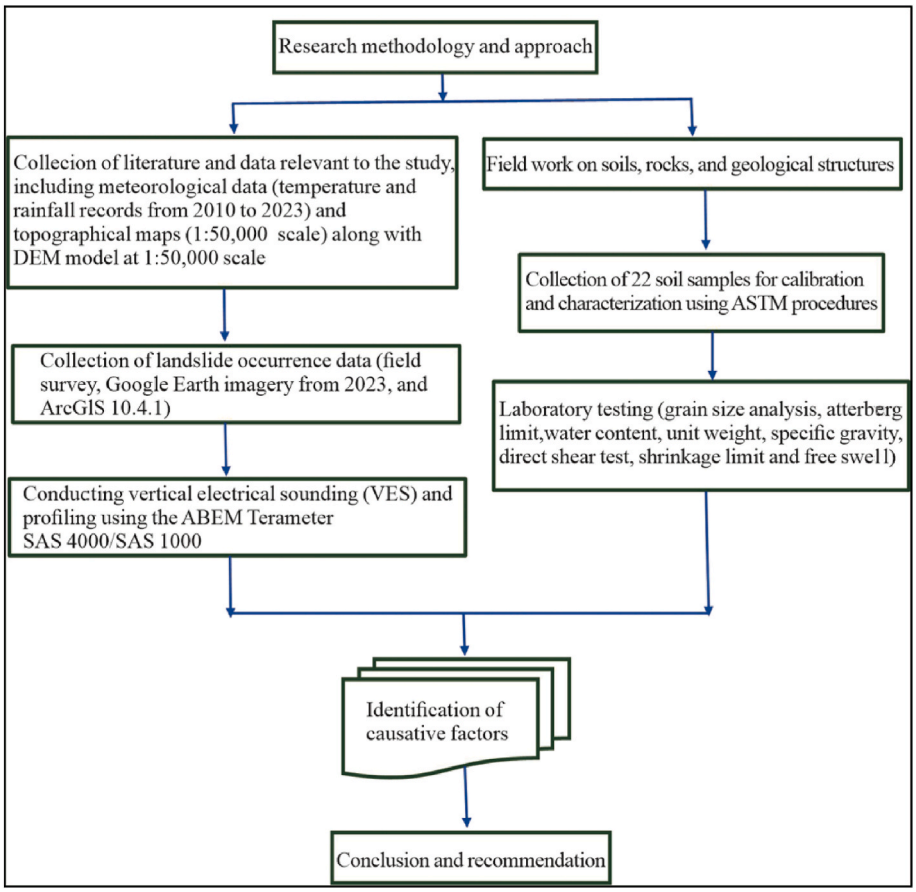


**Fig. 18.** Flow chart of the methodological framework.

### 3.3. Vertical electrical sounding (VES)

Vertical electrical soundings were used to examine the vertical layering and roughly identify the horizontally placed strata. An ABEM Terrameter SAS 4000/SAS 1000 with steel electrodes, wires on reels, and additional equipment were used to gather the electrical resistivity data (Fig. 17). Four electrodes were placed on the ground in a straight line. Two potential electrodes (M and N) were used to monitor the voltage changes that resulted from injecting current into the earth through electrodes A and B. Using the Schlumberger array (AMNB), the current electrodes were five times farther apart than the voltage electrodes. Profile lines with AB/2 and MN/2 spacing ranging from 1.5 to 220 and 0.5–20 m, respectively, were used for the VES. Along the sliding zone, profiling was also done at 10 m intervals perpendicular to the geological alignment, ranging from 0 to 230 m. To create a resistivity-depth model for iteration on the IPI2win software, the apparent resistivity (ρa) measurements were plotted against the electrode spacing (AB/2) (IP2win, 2008). After an RMS error of less than 5 % was achieved, iterations were completed. In this study, the ultimate RMS error is 3.52 %. Finally, a qualitative interpretation of the findings is presented. The effects of various geological materials within the area were demonstrated using the observed potential differences. IPI2win software was used to depict the raw resistivity data as a pseudo-depth section, showing the vertical variation of the recorded resistivity as a function of electrode spacing (AB/2). Alonso-Pandavenes et al. [24] used the VES method for landslide cause identification.

Fig. 18 shows the flow chart of the methodological framework used in the study.

**Table 2**
Classification of Lesalso, Aksum soils.

| Ser. No. | Test pit designation | Depth of sampling (m) | Percentage amount of particle size (%) | | | | LL (%) | PL (%) | PI (%) | Soil classification | | |
|---|---|---|---|---|---|---|---|---|---|---|---|---|
| | | | Gravel | Sand | Silt | Clay | | | | USC | ASHTO | Textural |
| 1 | RH-22 | 1.5 | | 13.3 | 40.2 | 46.5 | 47 | 23 | 24 | CL | A-7-6(22) | Silty clay |
| 2 | Du-19 | 1.5 | | 13.0 | 54 | 23 | 52 | 26 | 24 | CH | A-7-6(20) | Silty loam |
| 3 | Du-18 | 2.0 | | 57.5 | 35.2 | 7.3 | 49 | 30 | 19 | SC | A-2-7(2) | Sandy loam |
| 4 | La-4 | 1.5 | | 10.0 | 51.3 | 38.7 | 62 | 26 | 36 | CH | A-7-6(37) | Silty clay loam |
| 5 | Ls-11 | 2.5 | | 8.3 | 40.2 | 51.4 | 72 | 25 | 47 | CH | A-7-6(49) | Silty clay |
| 6 | Ls-9 | 1.5 | 3.4 | 23.7 | 40.3 | 32.6 | 37 | 16.05 | 20.95 | CL | A-6(19) | Clay loam |
| 7 | Rh-21 | 1.5 | | 8.0 | 67 | 25 | 55 | 34 | 21 | MH | A-7-5(37) | Silt loam |
| 8 | MAK-10 | 2.0 | 2.3 | 63.0 | 22 | 12.7 | 35.5 | 20.23 | 15.27 | SC | A-2-6(1) | Sandy loam |
| 9 | Msh-17 | 1.5 | | 52.2 | 38.4 | 9.4 | 49.5 | 36 | 13.6 | SM | A-2-7(1) | Sandy loam |
| 10 | Rh-23 | 1.5 | 4.3 | 59 | 21 | 15.7 | 66 | 49 | 17 | SM | A-2-7(2) | Sandy loam |
| 11 | Ls-8 | 2.0 | | 27.8 | 51.6 | 20.6 | 49 | 20.5 | 28.5 | CL | A-7-6(20) | Silt loam |
| 12 | Msh-1 | 2.0 | 1.2 | 58.3 | 33 | 7.5 | 46 | 31 | 15 | SM | A-2-7(1) | Sandy loam |
| 13 | La-6 | 2.5 | 2.7 | 38.3 | 35.6 | 23.4 | 48.3 | 21.7 | 26.6 | CL | A-7-6(13) | Loam |
| 14 | Ls-12 | 2.0 | | 10.3 | 38.1 | 51.6 | 72.4 | 22.75 | 49.65 | CH | A-7-6(49) | Clay |
| 15 | Ls-14 | 2.0 | | 18.7 | 62 | 19.3 | 58 | 25 | 33 | CH | A-7-6(29) | Silt loam |
| 16 | Du-20 | 1.5 | 1.8 | 52 | 18.2 | 28 | 39 | 22 | 17 | SC | A-2-6(2) | Sandy clay loam |
| 17 | Msh-2 | 1.5 | | 24 | 33 | 43 | 55 | 29 | 26 | CH | A-7-6(21) | Clay |
| 18 | Ls-5 | 2.0 | | 11 | 67.8 | 21.2 | 59.51 | 26.75 | 32.76 | CH | A-7-6(33) | Silt loam |
| 19 | Ls-16 | 2.0 | | 17 | 25 | 58 | 66 | 26 | 40 | CH | A-7-6(36) | Clay |
| 20 | Ls-13 | 2.5 | | 16 | 60 | 24 | 62 | 24 | 38 | CH | A-7-6(35) | Silt loam |
| 21 | Ls-15 | 1.5 | | 19 | 35 | 46 | 56 | 23 | 33 | CH | A-7-6(28) | Clay |
| 22 | Msh-3 | 1.5 | 2.7 | 36.3 | 43 | 18 | 48 | 29 | 19 | ML | A-7-6(10) | Loam |

Notes: LL is the liquid limit; PL is the plastic limit; USC is the unified soil classification; SM is the silty sand; CL/CI is the lean clay; MH is the elastic silt; and SC is the clayey sand.

## 4. Results

### 4.1. Soil laboratory test results

The clay fraction (CF) ranges from 7.3 % to 58 %. The silt fraction ranges from 18.2 % to 67 %, while the sand fraction ranges from 8 % to 63 %, and the gravel fraction is 0–4.3 % (Table 2).

The study revealed that 27.27 % of the soils were sandy with silt and clay, while 72.72 % were composed of fine-grained clay and silt particles. The measured *LL*, *PL* and *PI* of the studied 22 soil samples were variable. The *LL* ranged from 29.5 to 66.4 % (average of 47.83 %), *PL* from 16.05 % to 49 % (median of 26.635 %) and *PI* ranged from 7.6 % to 43.65 % (median of 21.1968 %) (Table 2). Similar techniques and findings have been produced by Jazouli et al. [25]. The *LL*, *PL*, and *PI* for the 16 (72.72 %) fine-grained soil samples ranged from 31 % to 66.4 %, 16.05 %–34 %, and 13 %–43.65 %, respectively (Table 2). The average plasticity index of the silt soils in the region is 39.3 %. According to the findings of the Atterberg limit test, the USCS classification system determined three of the sixteen fine-grained soils were low plastic silty (ML), four were lean clay (CL), and ten were clay (CH) (Fig. 19).

Consequently, clay accounted for 63.63 % of the area soils with values ranging from 7.3 % to 58 %. As shown in Table 2, the remaining six coarse soils were categorized as silty sands (SM) and clayey sands (SC). Kamal et al. [26] has reached similar results. According to the ASHTO soil classification, 14 of the area's soils were categorized as A-7-6, A-2-7, and A-2-4; the remaining soils were categorized as A-2-5,

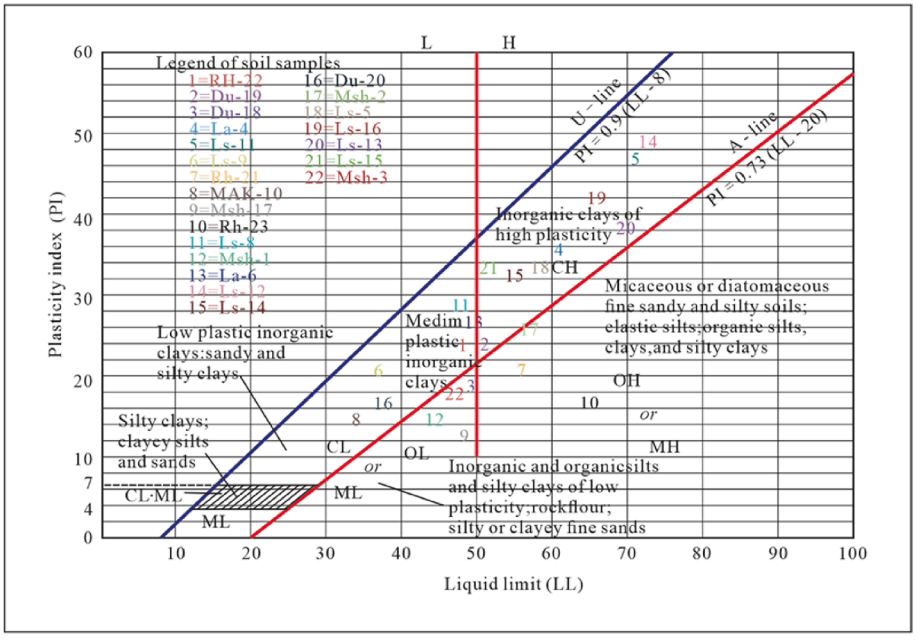


**Fig. 19.** Classification of the fine-grained Lesalso, Aksum soils using the USCS plasticity chart.

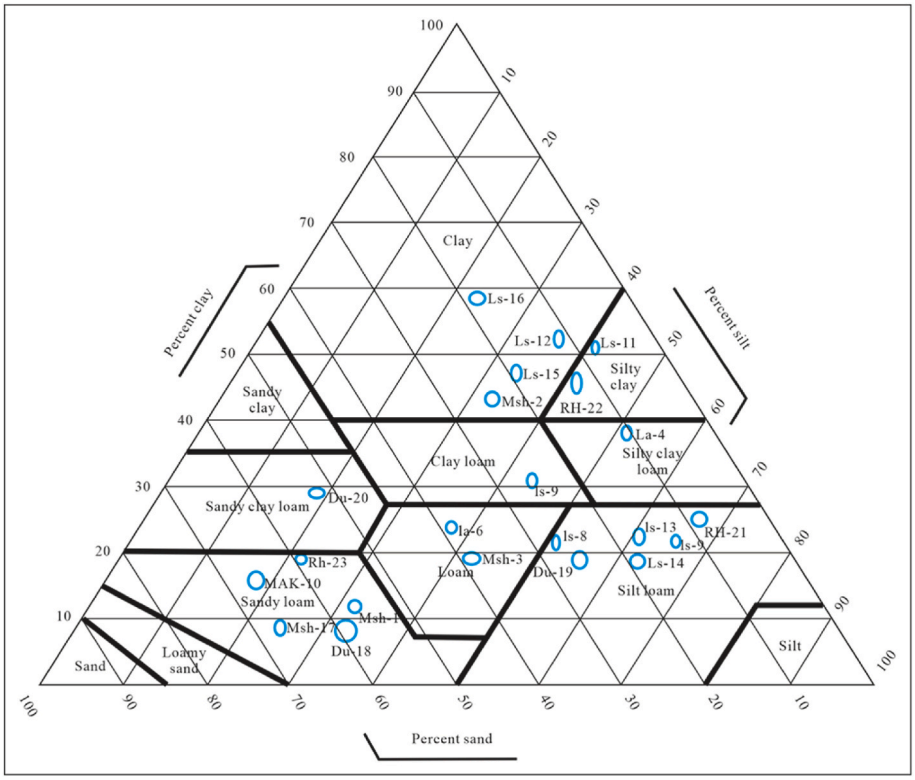


**Fig. 20.** Textural soil classification of Lesalso, Aksum soils.

A-2-6, A-7-5, and A-6 (Table 2). Similar results have been reported by Falowo and Aliu [27].

In the study area, soils were categorized by texture as clay, clay loam, loam, silt clay, silt loam, sandy loam, and sandy clay loam (Fig. 20). Berhane [28] has named soils similarly. As a result, 27.3 % of the soils in the area were coarse, while 72.7 % of the soils were fine.

Free swell values in the study area varied from 0.08 % to 71.5 %, averaging 33.29 % (Table 3).

The research area's water content measured values, which represented conditions during the dry season, ranged from 21 % to 54.3 % with an average of 36.02 % (Table 4). Similar findings were drawn by Tamiru et al. [31]. In particular, the water content of clay soils ranges from 32.11 % to 54.3 % with an average of 41.9 %, silt soils range from 32 % to 37.11 % with an average of 33.7 %, and sandy clay/silt soils range from 21 % to 30.98 % with an average of 24.5 % (Table 4).

The weight of a substance divided by the weight of an equivalent volume of water is known as its specific gravity. The average specific gravity of the soils examined was 2.66 %, with values ranging from 2.45 % to 2.81 % (Table 4).

The compression index of the soils ranges from 0.1785 % to 0.4368 %.

Table 5 shows the result of the collapsibility index ($K$) of Lesalso, Aksum soils. The collapsibility index for the areas' soils falls between −1.5 and −0.23.

The shrinkage limit test results range from 0.062 % to 30.86 % with a median of 12.9 % (Table 6). Similar results have been reported by Sridharan and Prakash [33]. The results of the shrinkage index, liquidity index, and consistency index tests were also determined, as presented in Table 6. The liquidity index values of soils in the study area are 0.225 % on average, as shown in Table 6, which is in a plastic state with intermediate strength.

The activity test result of the research area soils ranged from 0.379 % to 1.78 %, which is 0.8468 % on average (Table 7). The dry unit weight values varied from 1.467 to 2.254 g/cm$^3$ (Table 7).

Soil cohesion of the study area ranged from 6.45 to 52.72 kPa, with an average of 24.78 kPa (Table 8). The angle of internal friction obtained from the analyzed soil samples ranged between 7.68° and 47.94°, averaging 22.1° (Table 8).

### 4.2. Geophysical test

Vertical electrical soundings (VES) were conducted along the deep-seated landslide to trace the orientation and location of the geological contacts, which can have a considerable effect on the cause of the landslide (Fig. 21).

The VES interpretation of the profile line is based on lithological outcrops, surface observations, and the overall geological setup of the area (Fig. 22).

The upper layer with a thickness of 2.01 m and resistivity of 9.93 8 Ω·m is interpreted as topsoil with dry, strong basaltic rock fragments. The second layer, having a resistivity response of 1.5 8 Ω·m and a thickness of 1.48 m, is interpreted as a moist, soft to weak, fine/clay-dominant colluvium/alluvium deposit (highly to completely weathered basaltic materials); possibly it is a displaced (deformed) material due to the landslide (minor failure surfaces) (Table 9).

The third layer, which has shown a resistivity range of 10.8 Ω·m, is the highly to completely weathered basalt with slightly strong rock fragments (coarser materials); it could also be considered as an unstable zone, where the main failure surface is expected to exist. The fourth layer, with a resistivity of 86.28 Ω·m and 25.3 m thickness, is relatively medium to strong moderately weathered basalt (agglomeratic basalt), serving as a basal plane (strong) for the landslide. The fifth layer, with a resistivity of 8.478 Ω·m and having a substratum thickness, is attributed to highly to completely weathered basalt with slightly strong rock fragments (corestones) having moist to wet water conditions (Fig. 23).

Deep-seated failures within the study area's aphanitic basaltic rock unit were triggered by rainfall and due to the presence of spring.

**Table 3**
Relationship between swelling potential and degree of swell.

| Ser. No. | Test pit designation | Depth of sampling (m) | Liquid limit (%) | Plasticity index (PI) (%) | Swelling potential (SP) (%) | Degree of swell [29] | Degree of expansion [30] |
|---|---|---|---|---|---|---|---|
| 1 | RH-22 | 1.5 | 47 | 24 | 51.3 | High | High |
| 2 | Du-19 | 1.5 | 52 | 24 | 51.3 | High | High |
| 3 | Du-18 | 2.0 | 49 | 19 | 40.8 | Medium | High |
| 4 | La-4 | 1.5 | 62 | 36 | 76.5 | Very high | Very high |
| 5 | Ls-11 | 2.5 | 72 | 47 | 91.5 | Very high | Very high |
| 6 | Ls-9 | 1.5 | 37 | 20.95 | 44.895 | High | Medium |
| 7 | Rh-21 | 1.5 | 55 | 21 | 45 | High | High |
| 8 | MAK-10 | 2.0 | 35.5 | 15.27 | 32.967 | Medium | Medium |
| 9 | Msh-17 | 1.5 | 49.5 | 13.6 | 29.46 | Medium | High |
| 10 | Rh-23 | 1.5 | 66 | 17 | 36.6 | Medium | Very high |
| 11 | Ls-8 | 2.0 | 49 | 28.5 | 60.75 | High | High |
| 12 | Msh-1 | 2.0 | 46 | 15 | 32.4 | Medium | High |
| 13 | La-6 | 2.5 | 48.3 | 26.6 | 56.76 | High | High |
| 14 | Ls-12 | 2.0 | 72.4 | 49.65 | 94.16 | Very high | Very high |
| 15 | Ls-14 | 2.0 | 58 | 33 | 70.2 | High | High |
| 16 | Du-20 | 1.5 | 39 | 17 | 36.6 | Medium | Medium |
| 17 | Msh-2 | 1.5 | 55 | 26 | 55.5 | High | High |
| 18 | Ls-5 | 2.0 | 59.51 | 32.76 | 69.696 | High | High |
| 19 | Ls-16 | 2.0 | 66 | 40 | 84.9 | Very high | Very high |
| 20 | Ls-13 | 2.5 | 62 | 38 | 80.7 | Very high | Very high |
| 21 | Ls-15 | 1.5 | 56 | 33 | 70.2 | High | High |
| 22 | Msh-3 | 1.5 | 48 | 19 | 40.8 | Medium | High |

**Table 4**
Water content, compression index, and specific gravity test result.

| Ser. No. | Test pit designation | Depth of sampling (m) | Water content (%) | Compression index (%) | Specific gravity |
|---|---|---|---|---|---|
| 1 | RH-22 | 1.5 | 32.53 | 0.259 | 2.73 |
| 2 | Du-19 | 1.5 | 33.08 | 0.294 | 2.70 |
| 3 | Du-18 | 2.0 | 28.6 | 0.273 | 2.68 |
| 4 | La-4 | 1.5 | 45.92 | 0.364 | 2.70 |
| 5 | Ls-11 | 2.5 | 51.9 | 0.434 | 2.45 |
| 6 | Ls-9 | 1.5 | 32.11 | 0.189 | 2.51 |
| 7 | Rh-21 | 1.5 | 32.04 | 0.315 | 2.67 |
| 8 | MAK-10 | 2.0 | 21 | 0.1785 | 2.81 |
| 9 | Msh-17 | 1.5 | 30.98 | 0.2765 | 2.73 |
| 10 | Rh-23 | 1.5 | 22 | 0.392 | 2.74 |
| 11 | Ls-8 | 2.0 | 33 | 0.273 | 2.67 |
| 12 | Msh-1 | 2.0 | 23 | 0.252 | 2.56 |
| 13 | La-6 | 2.5 | 34 | 0.2681 | 2.70 |
| 14 | Ls-12 | 2.0 | 54.3 | 0.4368 | 2.54 |
| 15 | Ls-14 | 2.0 | 40.5 | 0.336 | 2.85 |
| 16 | Du-20 | 1.5 | 21.57 | 0.203 | 2.71 |
| 17 | Msh-2 | 1.5 | 37.11 | 0.315 | 2.78 |
| 18 | Ls-5 | 2.0 | 43.7 | 0.34657 | 2.7 |
| 19 | Ls-16 | 2.0 | 50.68 | 0.392 | 2.58 |
| 20 | Ls-13 | 2.5 | 49.5 | 0.364 | 2.78 |
| 21 | Ls-15 | 1.5 | 42.9 | 0.322 | 2.69 |
| 22 | Msh-3 | 1.5 | 32 | 0.226 | 2.67 |

## 5. Discussion

### 5.1. Soil properties and landslide occurrence

Soils with $PI>32.9$ % are susceptible to shrink-swell cycles, a known precursor to slope instability. Accordingly, 36.36 % of the area soils are susceptible to landslide [35]. Low degree of expansion is defined as soils with a free swell of less than 50 % [36]. Accordingly, 59.09 % of the study's soils have >50 % of free swell. Because of their distinct shrink-swell characteristics, problem soils have been shown to cause landslides at varying moisture contents [37].

Soils with water content exceeding 9.9 % are more susceptible to volumetric changes and potential failure [32]. Accordingly, all the soil samples are susceptible to volumetric variations and a possible failure.

Clay and silty clay soils, with specific gravity values ranging from 2.67 to 2.90, are prone to landslides due to their weak strength when

**Table 5**
Result of the Collapsibility index ($K$) of Lesalso, Aksum soils.

| Ser. No. | Test pit designation | Depth of sampling (m) | Collapsibility index ($K$) | Collapsing state [32] |
|---|---|---|---|---|
| 1 | RH-22 | 1.5 | −0.6 | Highly collapsible |
| 2 | Du-19 | 1.5 | −0.73 | Highly collapsible |
| 3 | Du-18 | 2.0 | −1.074 | Highly collapsible |
| 4 | La-4 | 1.5 | −0.45 | Highly collapsible |
| 5 | Ls-11 | 2.5 | −0.43 | Highly collapsible |
| 6 | Ls-9 | 1.5 | −0.23 | Highly collapsible |
| 7 | Rh-21 | 1.5 | −1.09 | Highly collapsible |
| 8 | MAK-10 | 2.0 | −0.95 | Highly collapsible |
| 9 | Msh-17 | 1.5 | −1.37 | Highly collapsible |
| 10 | Rh-23 | 1.5 | −2.6 | Highly collapsible |
| 11 | Ls-8 | 2.0 | −0.56 | Highly collapsible |
| 12 | Msh-1 | 2.0 | −1.5 | Highly collapsible |
| 13 | La-6 | 2.5 | −0.54 | Highly collapsible |
| 14 | Ls-12 | 2.0 | −0.365 | Highly collapsible |
| 15 | Ls-14 | 2.0 | −0.53 | Highly collapsible |
| 16 | Du-20 | 1.5 | −1.025 | Highly collapsible |
| 17 | Msh-2 | 1.5 | −0.69 | Highly collapsible |
| 18 | Ls-5 | 2.0 | −0.48 | Highly collapsible |
| 19 | Ls-16 | 2.0 | −0.383 | Highly collapsible |
| 20 | Ls-13 | 2.5 | −0.33 | Highly collapsible |
| 21 | Ls-15 | 1.5 | −0.397 | Highly collapsible |
| 22 | Msh-3 | 1.5 | −0.84 | Highly collapsible |

**Table 6**
Result of shrinkage limit, shrinkage index, liquidity index, and consistency index.

| Ser. No. | Test pit designation | Depth of sampling (m) | Shrinkage limit (%) | Shrinkage index (%) | Liquidity index (%) | Consistency index (%) | Description [34] |
|---|---|---|---|---|---|---|---|
| 1 | RH-22 | 1.5 | 14.76 | 8.24 | 0.397 | 0.603 | Medium stiff |
| 2 | Du-19 | 1.5 | 12.78 | 13.22 | 0.295 | 0.788 | Stiff |
| 3 | Du-18 | 2.0 | 19.63 | 10.37 | −0.0736 | 1.073 | Semi solid |
| 4 | La-4 | 1.5 | 6.52 | 19.48 | 0.555 | 0.445 | Soft |
| 5 | Ls-11 | 2.5 | 0.9 | 24.1 | 0.572 | 0.427 | Soft |
| 6 | Ls-9 | 1.5 | 15.78 | 0.27 | 0.7665 | 0.233 | Very soft |
| 7 | Rh-21 | 1.5 | 15.95 | 18.05 | −0.0933 | 1.093 | Semi solid |
| 8 | MAK-10 | 2.0 | 19.78 | 0.45 | 0.0504 | 0.94957 | Stiff |
| 9 | Msh-17 | 1.5 | 30.86 | 5.14 | −0.369 | 1.369 | Semi solid |
| 10 | Rh-23 | 1.5 | 20.39 | 28.61 | −1.588 | 2.588 | Semi solid |
| 11 | Ls-8 | 2.0 | 13.36 | 7.14 | 0.43859 | 0.561 | Medium stiff |
| 12 | Msh-1 | 2.0 | 22.78 | 8.22 | −0.533 | 1.533 | Semi solid |
| 13 | La-6 | 2.5 | 11.85 | 9.85 | 0.462 | 0.537 | Medium stiff |
| 14 | Ls-12 | 2.0 | 0.062 | 22.688 | 0.635 | 0.3645 | Soft |
| 15 | Ls-14 | 2.0 | 9.86 | 15.14 | 0.4696 | 0.53 | Medium stiff |
| 16 | Du-20 | 1.5 | 20.41 | 2.49 | −0.0253 | 1.025 | Semi solid |
| 17 | Msh-2 | 1.5 | 10.67 | 18.33 | 0.3119 | 0.688 | Medium stiff |
| 18 | Ls-5 | 2.0 | 7.76 | 18.99 | 0.5174 | 0.483 | Soft |
| 19 | Ls-16 | 2.0 | 1.07 | 24.93 | 0.617 | 0.383 | Soft |
| 20 | Ls-13 | 2.5 | 3.45 | 20.55 | 0.671 | 0.3289 | Soft |
| 21 | Ls-15 | 1.5 | 8.65 | 14.35 | 0.603 | 0.3969 | Soft |
| 22 | Msh-3 | 1.5 | 16.71 | 12.29 | 0.1578 | 0.842 | Stiff |

**Table 7**
Activity of soils and dry unit weight (g/cm$^3$) of Lesalso, Aksum soils result.

| Ser. No. | Test pit designation | Depth of sampling (m) | Activity of soils (%) | Soil name definition [34] | Dry unit weight (g/cm$^3$) |
|---|---|---|---|---|---|
| 1 | RH-22 | 1.5 | 0.52 | In active | 1.766 |
| 2 | Du-19 | 1.5 | 1.04 | Normal | 1.767 |
| 3 | Du-18 | 2.0 | 2.6 | Active | 1.802 |
| 4 | La-4 | 1.5 | 0.93 | Normal | 1.804 |
| 5 | Ls-11 | 2.5 | 0.91 | Normal | 2.249 |
| 6 | Ls-9 | 1.5 | 0.64 | In active | 2.254 |
| 7 | Rh-21 | 1.5 | 0.84 | Normal | 1.802 |
| 8 | MAK-10 | 2.0 | 1.2 | Normal | 1.766 |
| 9 | Msh-17 | 1.5 | 1.4 | Active | 1.767 |
| 10 | Rh-23 | 1.5 | 1.08 | Normal | 2.249 |
| 11 | Ls-8 | 2.0 | 1.38 | Active | 1.802 |
| 12 | Msh-1 | 2.0 | 2.0 | Active | 1.508 |
| 13 | La-6 | 2.5 | 1.1 | Normal | 1.804 |
| 14 | Ls-12 | 2.0 | 0.96 | Normal | 2.254 |
| 15 | Ls-14 | 2.0 | 1.709 | Active | 1.467 |
| 16 | Du-20 | 1.5 | 0.607 | Inactive | 1.748 |
| 17 | Msh-2 | 1.5 | 0.604 | Inactive | 1.883 |
| 18 | Ls-5 | 2.0 | 1.54 | Active | 1.467 |
| 19 | Ls-16 | 2.0 | 0.68 | Inactive | 2.254 |
| 20 | Ls-13 | 2.5 | 1.58 | Active | 1.883 |
| 21 | Ls-15 | 1.5 | 0.71 | Inactive | 1.467 |
| 22 | Msh-3 | 1.5 | 1.05 | Normal | 1.748 |

**Table 8**
Cohesion and internal friction angle results of the Lesalso, Aksum soils.

| Ser. No. | Test pit designation | Depth of sampling (m) | Cohesion (kPa) | Internal friction angle (°) |
|---|---|---|---|---|
| 1 | RH-22 | 1.5 | 20.07 | 15.73 |
| 2 | Du-19 | 1.5 | 13.67 | 7.68 |
| 3 | Du-18 | 2.0 | 40.72 | 39.72 |
| 4 | La-4 | 1.5 | 34.63 | 14.81 |
| 5 | Ls-11 | 2.5 | 19.73 | 16.91 |
| 6 | Ls-9 | 1.5 | 11.75 | 11.62 |
| 7 | Rh-21 | 1.5 | 36.83 | 18.01 |
| 8 | MAK-10 | 2.0 | 52.72 | 43.72 |
| 9 | Msh-17 | 1.5 | 43.73 | 31.74 |
| 10 | Rh-23 | 1.5 | 34.72 | 40.72 |
| 11 | Ls-8 | 2.0 | 10.45 | 10.32 |
| 12 | Msh-1 | 2.0 | 38.72 | 35.72 |
| 13 | La-6 | 2.5 | 8.95 | 13.9 |
| 14 | Ls-12 | 2.0 | 17.37 | 19.3 |
| 15 | Ls-14 | 2.0 | 18.38 | 21.9 |
| 16 | Du-20 | 1.5 | 40.93 | 47.94 |
| 17 | Msh-2 | 1.5 | 14.21 | 12.32 |
| 18 | Ls-5 | 2.0 | 21.57 | 14.23 |
| 19 | Ls-16 | 2.0 | 12.54 | 17.83 |
| 20 | Ls-13 | 2.5 | 25.37 | 9.33 |
| 21 | Ls-15 | 1.5 | 22.41 | 18.52 |
| 22 | Msh-3 | 1.5 | 6.45 | 24.32 |

saturated with water [38]. As a result, 72.72 % of the study's soils had a specific gravity of >2.67. Soil specific gravity values between 2.65 and 2.84 are common, indicating a predominant presence of clay and silty clay materials, which are significant in landslide occurrences [31]. In the research area, 54.54 % of the soils have a specific gravity of less than 2.7, making them easily prone to sliding.

According to study by Casagrande [39], 54.55 % of the area's soils have intermediate compressibility, 40.909 % high, and 4.55 % low (Table 4).

Based on $K$ values, soils were classified as highly collapsible ($K < 0.5$), marginally collapsible ($0<K \leq 0.5$), or a non-collapsing ($K > 0.5$) [32]. According to study by Tchuwa and Makande [32], all soils at the site exhibit high collapsibility (Table 5).

According to Kalikin [40], for $LI < 0$, the soil will have high strength and, with a semisolid state, if $0<LI < 1$, the soil is in a plastic state with intermediate strength, and if $LI > 1$, the soils are in a liquid state with very low strength. Soils with a low liquidity index ($LI < 0$) are typically more brittle and dry.

In terms of potential expansiveness, soils with activity less than 0.75 are low, 0.75–1.25 are medium, and those with greater than 1.25 are highly expansive [28]. In the study area, 40.9 % of the soil samples are low, 27.3 % are medium, and 31.8 % are highly expansive. Highly active soils have been found to be prone to deep cracks and abrupt loss of strength, which could result in shallow landslides [41].

An increase in unit weight, such as that caused by water infiltration, increases driving forces and lowers the safety factor (FOS), increasing the slope's susceptibility to failure [42].

Cohesion values ranging from 0.0 to 0.4 kg/cm$^2$ are the main cause of landslides, with lower values (e.g. 0.0–0.2 kg/cm$^2$) showing more vulnerability [43]. Accordingly, >50 % of the soils in the area had low cohesion values, which raised the likelihood of landslides.

### 5.2. Geophysical test and landslide occurrence

The alteration of basalt creates weak interlayers that can

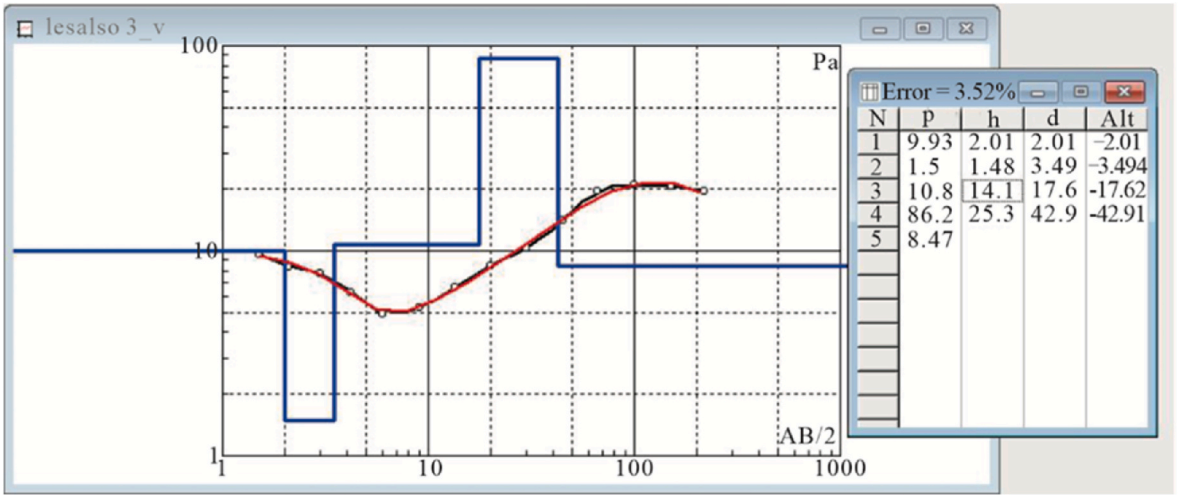


**Fig. 21.** Profiling images varying resistivity layers, which indicates indicative of different lithological formations (GPS: X: 478802 mE, Y: 1564266 mN, Z: 2109 m.asl (Zone 37N)).

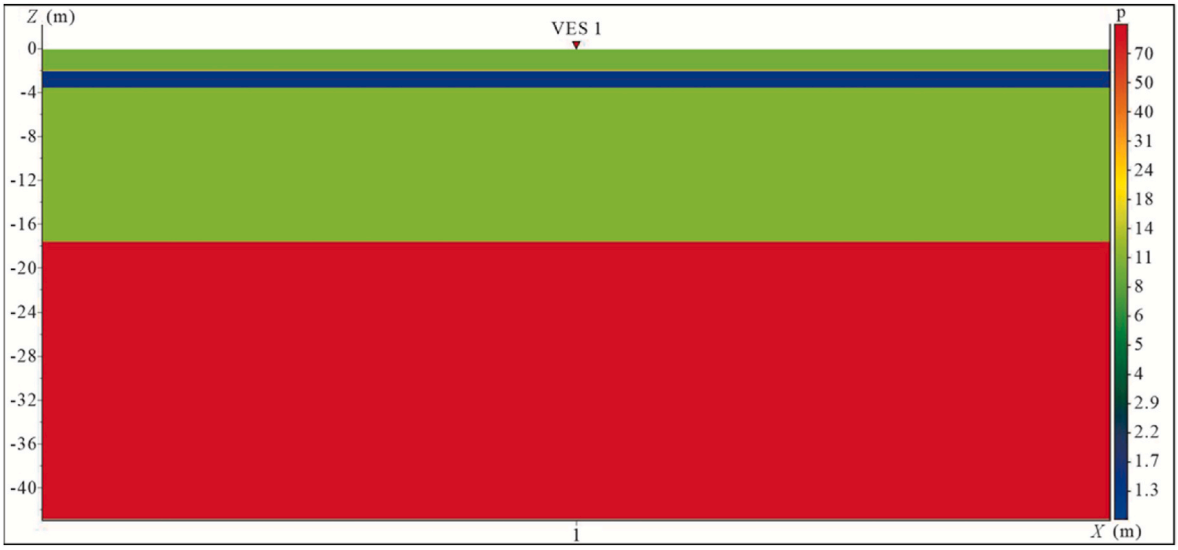


**Fig. 22.** Apparent resistivity pseudo-depth section map along profile line 1.

significantly reduce slope stability, especially when saturated with water [44]. This layer has a lower resistivity value than that of the overlying layer and is associated with the water-bearing fractured basalt. Upon contact with water, the weak interlayer will exhibit pronounced weakening of its strength, making the slope prone to sliding along the weak layer [41]. The classification of the highly to completely weathered basalt with slightly strong rock fragments layer as a potential slip surface is grounded in the fact that this layer exhibits low levels of porosity and permeability. This characteristic hinders the movement of water. Consequently, the increasing load due to water accumulation diminishes the cohesion and friction, thereby elevating the potential for landslides. The decrease in shear strength is also affected by higher pore pressure within the weathered basalt layer [45]. Geological unit resistivity rises with increasing depth [46]. However, its value decreases at the fifth layer, characterised by highly to completely weathered basalt containing slightly strong rock fragments (corestones), and a moist to wet unit. The reduced strength of the rock unit is attributed to the presence of a thin layer of moist to wet basalt.

Previous research by Tang et al. [47] suggests that rainfall, particularly prolonged heavy rain, is a primary cause of landslides on basalt platforms. Though triggered by rainfall, the landslide is believed to have been affected by various factors, which include long-term as well as short-term processes. The long-term processes involved a complex interaction of processes including the lubrication of soft rocks, weathering, and subsurface erosion (piping). Ng and Shi [48] analyzed the influence of different rainfall duration and intensity on the stability of an unsaturated soil slope and discussed the influence of different strata and rainfall conditions on the pore water pressure distribution of the slope. For subsurface study, VES is an inexpensive and non-destructive method [49]. However, VES data interpretation can be complex and may need to be combined with other geophysical and geotechnical methods [50].

## 6. Conclusions

The study conducted in Lesalso, central zone of northern Ethiopia, aimed to identify the causative and triggering factors of landslides. The research employed field investigations, soil laboratory analyses, VES and profiling methods. Physical and engineering properties of 22 soil samples indicated that the failure materials mainly consist of fine grain soils (72.72 %), liquid limit (29.5 %–66.4 %) and plasticity index (7.6 %–43.65 %), medium to high degree of swelling (0.08 %–71.5 %), variable low to high water content (21 %–54.3 %), specific gravity

**Table 9**
Profile line and interpretation from VES result.

| Layer number | Apparent resistivity $\rho$ (Ω·m) | Thickness (m) | Depth range (m) | Possible lithology (interpretation) |
|---|---|---|---|---|
| 1 | 9.93 | 2.01 | 0–2.01 | Topsoil with dry, strong rock fragments |
| 2 | 1.5 | 1.48 | 2.01–3.49 | Moist, soft to weak, fine/clay dominant colluvium/alluvium deposit (highly to completely weathered basaltic materials), possibly it is a displaced (deformed) material due to the landslide (minor failure surfaces) |
| 3 | 10.8 | 14.1 | 3.49-17.62 | Highly to completely weathered basalt with slightly strong rock fragments (coarser materials), it could also be considered as unstable zone, where the main failure surface expected to exist |
| 4 | 86.2 | 25.3 | 17.59-42.91 | Relatively medium to strong moderately weathered basalt (agglomeratic basalt), served as a basal plane (strong) for the landslide |
| 5 | 8.47 | Substratum | 42.91-? | Highly to completely weathered basalt with slightly strong rock fragments (corestones), moist to wet |

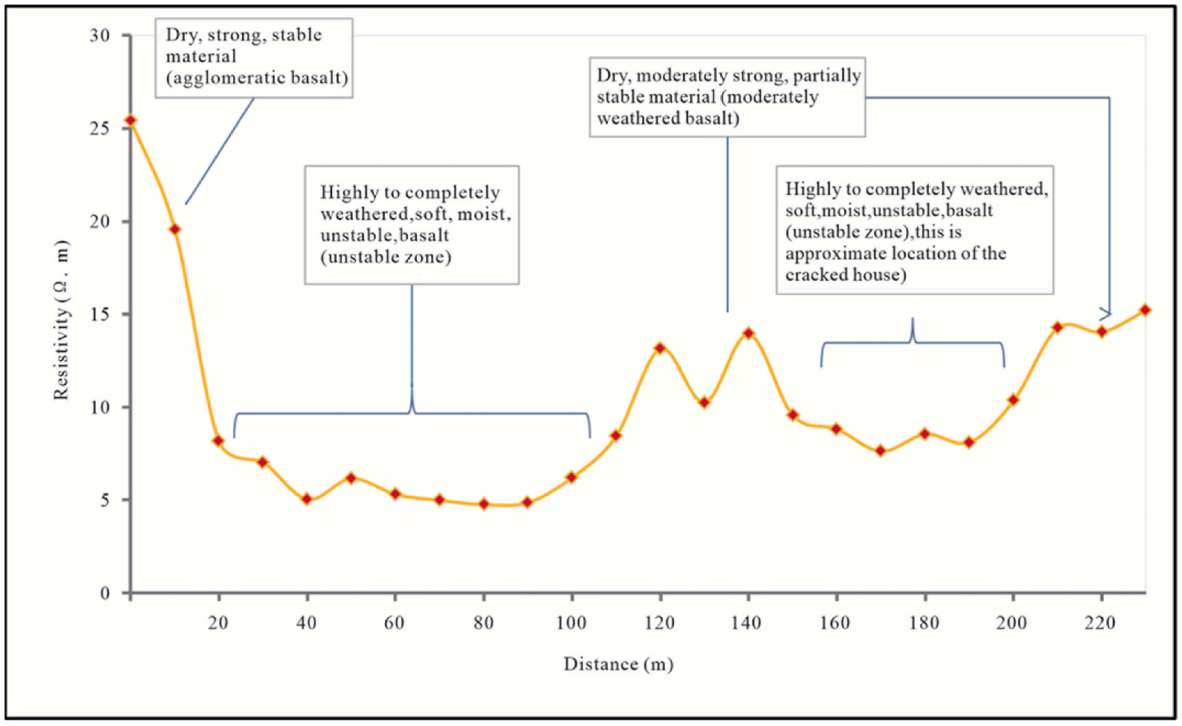


**Fig. 23.** Profile line one preliminary interpretation (GPS) of last reading (X: 478621 mE, Y: 1564187 mN, Z: 2124 m. a. s. l).

(2.45–2.81), dry unit weight (1.467 g/cm$^3$ to 2.254 g/cm$^3$), activity of soils (0.379 %–1.78 %), soil compression index (0.1785 %–0.43685 %), shrinkage index (0.27 %–28.61 %), shrinkage limit (0.062 %–30.86 %), friction angle $\phi$ (7.68°–47.94°) and cohesion $C$ (6.45 kPa–52.72 kPa). The subsurface geology of the failure section is grouped into topsoil with dry and strong rock fragments, moist, soft to weak, fine/clay dominant colluvium/alluvium deposit (highly to completely weathered basaltic), highly to completely weathered basalt with slightly strong rock fragments (coarser materials), relatively medium to strong moderately weathered basalt (agglomeratic basalt), highly to completely weathered basalt with slightly strong rock fragments (corestones), moist to wet units. The pseudo depth section map created for the site effectively illustrates the variations in apparent resistivity in both vertical and horizontal dimensions across the survey area. The on-site examination revealed that the aphanitic basalt rock in the failed section has undergone significant weathering and disturbance, resulting in its high permeability. Hence, it serves to recharge rainwater to down-slope. The stability of the large-scale landslide in the area is dominantly controlled by (1) the presence of hard, competent, and permeable rocks underlain by soft, incompetent, and impermeable rocks, (2) the presence of fine grain soils (clay and silt (3) A geohydrological environment (spring) which promotes water pressure build-up, and (4) A steep slope, which can mobilize adequate stress to promote failure. The findings of this study have important implications for landslide prevention and management in Lesalso and other regions with similar geological and topographical conditions.

## CRediT authorship contribution statement

**Abadi Gebrehiwot:** Writing – original draft, Conceptualization, Data curation. **Gebremedhin Berhane:** Methodology, Formal analysis, Investigation, Conceptualization. **Yewhalashet Fissha:** Validation, Visualization, Methodology. **Yemane Kide:** Writing – original draft, Formal analysis, Investigation. **Welegerima Teklay:** Visualization, Validation. **Belaynesh Mekonen:** Data curation, Conceptualization. **Enming Li:** Writing – review & editing, Supervision, Validation, Resources.

## Declaration of competing interest

The authors declare that they have no known competing financial interests or personal relationships that could have appeared to influence the work reported in this paper.

## Acknowledgements

Enming Li is supported by the China Scholarship Council (No. 202006370006).

## References


[1] Y. Alimohammadlou, A. Najafi, A. Yalcin, Landslide process and impacts: a proposed classification method, Catena 104 (2013) 219–232.
[2] K.T. Chau, Y.L. Sze, M.K. Fung, W.Y. Wong, E.L. Fong, L.C.P. Chan, Landslide hazard analysis for Hong Kong using landslide inventory and GIS, Comput. Geosci. 30 (4) (2004) 429–443.
[3] T. Mersha, M. Meten, GIS-based landslide susceptibility mapping and assessment using bivariate statistical methods in Simada area, northwestern Ethiopia, Geoenvironmental disasters 7 (2020) 1–22.
[4] B. Tesfaye, M. Jothimani, Z. Dawit, Mapping landslide susceptibility in the debretabor-alember road sector, Northwestern Ethiopia through geospatial tools and statistical approaches, Journal of Degraded & Mining Lands Management 11 (2) (2024) 5169–5179.
[5] M.P. Amarasinghe, S.A.S. Kulathilaka, D.J. Robert, A. Zhou, H.A.G. Jayathissa, Risk assessment and management of rainfall-induced landslides in tropical regions: a review, Nat. Hazards 120 (3) (2024) 2179–2231.
[6] X. Pei, S. Cui, L. Zhu, H. Wang, L. Luo, X. Zhang, Sanxicun landslide: an investigation of progressive failure of a gentle bedding slope, Nat. Hazards 111 (1) (2021) 51–78, 1-28.
[7] V. Agnesi, M. Camarda, C. Conoscenti, C. Di Maggio, I.S. Diliberto, P. Madonia, E. Rotigliano, A multidisciplinary approach to the evaluation of the mechanism that triggered the Cerda landslide (Sicily, Italy), Geomorphology 65 (1–2) (2005) 101–116.
[8] B. Yalcinalp, Z. Ogretmen Aydin, H. Ersoy, A. Seren, Investigation of geological, geotechnical and geophysical properties of Kiratli (Bayburt, NE Turkey) travertine, Carbonates Evaporites 33 (3) (2018) 421–429.
[9] R. Fell, O. Hungr, S. Leroueil, W. Riemer, Keynote lecture-geotechnical engineering of the stability of natural slopes, and cuts and fills in soil, in: ISRM International Symposium (Pp. ISRM-IS), ISRM, 2000 November.
[10] L. Ay, Hillside Settlements: the Case of May Liham, TIGRAY, 2022.
[11] O.P. Olabode, H.S. Lim, M.H. Ramli, Geophysical and geotechnical evaluation of landslide slip surface in a residual soil for monitoring of slope instability, Earth Space Sci. 9 (12) (2022), 2022EA002248.
[12] ENMSA (Ethiopian National Meteorology Service Agency), Daily Rainfall Data of Aksum Weather Station, Addis Ababa, Unpublished Report. (2010-2023).
[13] C. Natali, L. Beccaluva, G. Bianchini, F. Siena, The Axum–Adwa basalt–trachyte complex: a late magmatic activity at the periphery of the Afar plume, Contrib. Mineral. Petrol. 166 (2013) 351–370.
[14] S.B. Leulalem, W. Kifle, T. Nata, Geological and geotechnical investigations of Axum dam site, Tigray, Northern Ethiopia, International Journal of Scientific and Technology Research 5 (2016) 84–111.
[15] L.G. Teklebrhan, H. Zelealem, A.G. Daniel, Geotourism of axum and yeha monuments, Northern Ethiopia, Geo J. Tour. Geosites 48 (2) (2023) 685–695.
[16] S. Wendim, K. Woldearegay, G. Mebrahtu, Causes, Failure Mechanisms and Susceptibility Zonation of Landslides along Gedo-Dilb Road Corridor, Northern Ethiopian, 2023.
[17] Q. Meng, P. Confuorto, Y. Peng, F. Raspini, S. Bianchini, S. Han, H. Liu, N. Casagli, Regional recognition and classification of active loess landslides using two-dimensional deformation derived from Sentinel-1 interferometric radar data, Remote Sens. 12 (10) (2020) 1541.
[18] M. Baldwin, D. Gosling, BS EN ISO 22475-1, implications for geotechnical sampling in the UK, Ground Eng. 42 (8) (2009) 28–31.
[19] A.S.T.M. Standard, D4318, Standard Test Methods for Liquid Limit, Plastic Limit, and Plasticity Index of Soils, ASTM International, West Conshohocken, PA, 2017.
[20] D. 2. ASTM, Standard test methods for laboratory determination of water (moisture) content of soil and rock by mass, in: Am. Soc. Test, Mater, 2010, pp. 1–5.
[21] ASTM, Standard Test Methods for Specific Gravity of Soil Solids by the Water Displacement Method, ASTM, West Conshohocken, PA, 2023.
[22] British Standard, B.S., 1377-7, Methods of Test for Soils for Civil Engineering Purposes Part 7, Shear Strength Tests (Total Stress), British Standard Institution, London, UK, 1990.
[23] A. D3080-11, Standard test method for direct shear test of soils under consolidated drained conditions, in: Annual Book of ASTM Standards, ASTM Standards, USA, West Conshohocken, PA, 2003, p. 4.
[24] O. Alonso-Pandavenes, F.J. Torrijo, J. Garzón-Roca, A. Gracia, Early investigation of a landslide sliding surface by HVSR and VES geophysical techniques combined, a case study in Guarumales (Ecuador), Appl. Sci. 13 (2) (2023) 1023.
[25] A. El Jazouli, A. Barakat, R. Khellouk, Geotechnical studies for landslide susceptibility in the high basin of the Oum Er Rbia river (Morocco), Geology, Ecology, and Landscapes 6 (1) (2022) 40–47.
[26] A.M. Kamal, F. Hossain, M.Z. Rahman, B. Ahmed, P. Sammonds, Geological and soil engineering properties of shallow landslides occurring in the Kutupalong Rohingya Camp in Cox's Bazar, Bangladesh, Landslides 19 (2) (2022) 465–478.
[27] O.O. Falowo, A. Aliu, Geoengineering investigation of an erosion induced highway structural failure along Ifon-Benin highway, Southwestern Nigeria, Earth Sciences Malaysia 4 (1) (2020) 51–60.
[28] G. Berhane, Engineering geological soil and rock characterization in the Mekelle town, Northern Ethiopia: implications to engineering practice, Momona Ethiop J Sci. 2 (2) (2010) 64–86.
[29] H.B. Seed, R.J. Woodward Jr., R. Lundgren, Prediction of swelling potential for compacted clays, J. Soil Mech. Found Div. 88 (3) (1965) 53–87.
[30] F. Chen, Foundation on Expansive Soils, 1975.
[31] M. Tamiru, W.F. Kabeta, D. Tsige, H. Ware, T. Zeberga, Geotechnical analysis and stability assessment of a landslide event in Gera Woreda, Ethiopia, Cogent Eng. 11 (1) (2024) 2405745.
[32] I. Tchuwa, M. Makande, A Geotechnical Assessment of Collapsible and Dispersive Soils for Landslide Risk Evaluation: a Case Study of Soche Hill, Blantyre, Malawi, 2025.
[33] A. Sridharan, K. Prakash, Shrinkage limit of soil mixtures, Geotech. Test. J. 23 (1) (2000) 3–8.
[34] V. Murthy, Principles and Practices of Soil Mechanics and Foundation Engineering, Marcek Decker INC., New York, 2002.
[35] V.K. Thakur, D.N. Singh, Rapid determination of swelling pressure of clay minerals, J. Test. Eval. 33 (4) (2005) 239–245.
[36] T.T. Woldesenbet, T.G. Telila, F.F. Feyessa, Geotechnical and geological investigation of landslide in West Arsi zone, Ethiopia, Environ. Earth Sci. 82 (18) (2023) 427.
[37] A. Yalcin, A geotechnical study on the landslides in the Trabzon province, NE, Turkey, Appl. Clay Sci. 52 (1–2) (2011) 11–19.
[38] M. Das Braja, Soil Mechanics Laboratory Manual, Oxford University Press, 2016.
[39] A. Casagrande, Classification and identification of soils, Trans. Am. Soc. Civ. Eng. 113 (1) (1948) 901–930.
[40] V.N. Kalikin, Soil Mechanics, Calculation, Principle, and Methods, 2017.
[41] Z. Zhang, R. Zeng, X. Meng, S. Zhao, S. Wang, J. Ma, H. Wang, Effects of changes in soil properties caused by progressive infiltration of rainwater on rainfall-induced landslides, Catena 233 (2023) 107475.
[42] D.W. Apriani, U. Mustofa, R. Hidayat, Soil shear strength parameter analysis based on behavior analysis of landslide case, U KaRsT 4 (2) (2020) 163–176.
[43] P.B. Santoso, A. Apriyono, R. Suryani, Inverse distance weighting interpolated soil properties and their related landslide occurrences, in: MATEC Web of Conferences, EDP Sciences, vol. 195, 2018 03013.
[44] C. Zhang, Z. Li, C. Yu, B. Chen, M. Ding, W. Zhu, J. Yang, Z. Liu, J. Peng, An integrated framework for wide-area active landslide detection with InSAR observations and SAR pixel offsets, Landslides 19 (12) (2022) 2905–2923.
[45] M. Souisa, L. Hendrajaya, G. Handayani, Landslide hazard and risk assessment for Ambon city using landslide inventory and geographic information system, in: Journal of Physics, vol. 739, IOP Publishing, 2016 012078, 1.
[46] G. Mebrahtu, S. Atsbaha, B.A. Berhe, Vertical electrical sounding (VES) investigation for road failure along Mekelle–Abi-Adi road segment, northern Ethiopia, Momona Ethiopian Journal of Science 13 (1) (2021) 134–146.
[47] M. Tang, Q. Xu, H. Yang, S. Li, J. Iqbal, X. Fu, X. Huang, W. Cheng, Activity law and hydraulics mechanism of landslides with different sliding surface and permeability in the three gorges reservoir area, China, Eng. Geol. 260 (2019) 105212.
[48] C.W.W. Ng, Q. Shi, Influence of rainfall intensity and duration on slope stability in unsaturated soils, Q. J. Eng. Geol. Hydrogeol. 31 (2) (1998) 105–113.
[49] S. Yılmaz, Z. Kamacı, Resistivity and seismic refraction studies on kısıklı landslide (Antalya, Turkey), International Journal of Computational and Experimental Science and Engineering 4 (3) (2018) 9–14.
[50] A. Okeha, A. Mallama, O.A. Uyimwena, S.A. Ganiyu, Review of identified shortcomings in aquifer vulnerability assessments 7 (1) (2023) 20–29.